An Optimization Study on Resistance Spot Welding of DP600 Sheet Steel via Experiment and Statistical Analysis

Abdulkarim Alzahougi
Department of Mechanical Engineering, Faculty of Engineering, Karabuk University, Türkiye
aalzahougi@yahoo.com

Bilge Demir
Department of Mechanical Engineering, Faculty of Engineering, Karabuk University, Türkiye
bdemir@karabuk.edu.tr

Muhammed Elitas
Department of Mechanical Engineering, Faculty of Engineering, Bilecik Şeyh Edebali University, Türkiye
muhammed.elitas@bilecik.edu.tr (corresponding author)

Received: 22 February 2023 | Revised: 20 March 2023 | Accepted: 29 March 2023

 DOI: https://doi.org/10.48084/etasr.5804

ABSTRACT

Resistance Spot Welding (RSW) is widely used in many automotive, boiler, and ship manufacturing industries. Therefore, the optimization and effectiveness of the RSW process are very useful and cost-efficient processes in addition to improving weld quality. This study used various welding parameters to investigate the optimization of the RSW process of Advanced High Strength Steel (AHSS). RSW was carried out using different welding times, currents, and electrode pressure values. Microstructural analysis, nugget formation, and tensile shear test were performed on samples. This study applied the Taguchi method and ANOVA to set up the welding process and optimize its results. Microstructural characterization showed that the weld nugget microstructures had a high-volume fraction of martensite. Using the Minitab software, Taguchi (DOE) and ANOVA on the tensile shear test results showed that welding current is more effective than clamping pressure on the tensile shear load-bearing capacity (TLBC). However, clamping pressure affects the weld current effects on weld performance. Additionally, the TLBC of RSW samples increases, whereas increasing the clamping pressure leads to a decrease in TLBC and nugget dimensions. Consequently, a detailed analysis of the RSW coefficients and their effects led to optimized results.

Keywords-AHSS; resistance spot welding; tensile shear load bearing capacity; optimization

I. INTRODUCTION

The main objectives of the automotive industry are increased safety, reduced fuel consumption and weight, and improved comfort [1-2]. Advanced High-Strength Steel (AHSS) is the most suitable material for these purposes. AHSS is mostly joined with the RSW method, which has many advantages [3-4]. For this reason, academic and industrial research focuses on it [5-8]. In addition, many materials have been successfully welded and studied in detail on RSW so far [9-13]. Optimization is one of the most beneficial approaches to match the operational plan requirements of any engineering field, such as maximizing RSW process conditions and minimizing consumption, waste, and costs [14]. From the perspective of RSW, the optimum parameters provide ideal electricity consumption and nugget geometry conditions, resulting in minimum pressing force, electrode wear, excellent heat retention, and better mechanical properties [15]. The primary reason minimum temperatures are important is that excessive heat in the RSW weld zone has detrimental effects on electrode and material properties and energy losses [16]. In addition, increased power consumption causes environmental concerns and increased carbon emissions and poses serious economic and technological problems [17].

Several studies focused on the optimization of RSW. In [18], finite element analysis was used, while in [14] statistical analysis was applied. The importance of electrode pressure, electrode diameter, welding current, and welding time were highlighted in [15] but didn't mention tensile shear load-bearing capacity (TLBC) decreasing via increasing the weld

electrode clamping (EWC) pressure. However, this study reported that electrode pressure was the second most effective parameter after weld current. In [19], it was shown that welding time had a more significant effect on weld strength at low currents than at high currents, but there was no mention of EWC pressure. In [20] the mechanical properties of RSW on DP600-DP1000 sheet steels were studied, and in [6] the effects of welding time and electrode pressure on mechanical properties were investigated. In [21], the optimization of process parameters on the tensile shear strength was investigated in RSW steels.

In all these studies, there are differences in the materials used and the results. This study aimed to examine whether these differences arise from differences in practical applications to clear the effect of EWC on weld properties. Although many studies investigated the effect of RSW parameters on the mechanical properties of advanced sheet steel junctions, only a few studied the effects of electrode pressure, welding time, and welding current simultaneously [22-24]. Furthermore, optimization is rarely seen in these studies. This study used cost-effective optimization, the Taguchi method, and ANOVA to describe the effect of electrode pressure under different welding currents and time conditions in RSW.

II. EXPERIMENTAL AND OPTIMIZATION STUDIES

Commercial DP600 steel sheet in 250×250×1mm dimensions was supplied from TOFAŞ Otomotiv Inc. in Bursa, Türkiye, and Table I shows its chemical composition.

TABLE I. DP600 STEEL'S CHEMICAL COMPOSITION (WT.%)

C	Mn	Si	Cr	Al	Ni	S	V	Fe
0.078	1.92	0.264	0.177	0.11	0.021	0.006	0.004	97.472

Figure 1 shows the dimensions and the overlapping position of the RSW instance as a drawing, carried out according to EN ISO 14273.

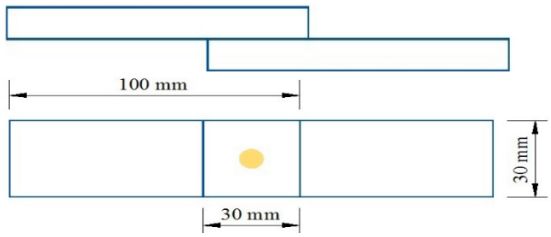

Fig. 1. The geometry of the overlapped sample of the DP600 sheet steel.

The size of the RSW overlapping samples was 170mm. Table II shows the different RSW parameters of the experiments. The RSW machine was AC and pneumatically controlled. Before welding, the surfaces of the test pieces were cleaned with methyl alcohol. Conical Cu-Cr alloy electrodes with an 8mm contact diameter were used in the welding process. These cross-section profiles of the RSW joint samples were prepared for optical microscopy microstructure analysis by applying standard metallographic procedures, such as grinding, polishing, and etching with a 2% nital solution.

TABLE II. RSW WELDING PARAMETERS

Electrode clamping pressure (bar)	Welding current (kA)	Welding time (s)
3.5	4, 6 & 8	0.3 & 0.5
4.5	4, 6 & 8	0.3 & 0.5
5.5	4, 6 & 8	0.3 & 0.5

A crosshead speed of 2 mm/min was applied in tensile shear tests, in the scope of DIN EN ISO 14272, using a SHIMADZU AGS-X Universal tensile test machine having 100 kN loading capacity. The RSW parameters were adjusted using the Taguchi method, as:

$$L27(3^2);\ Factors{:}\,2;\ Runs{:}\,27$$

Tensile-shear strength values were evaluated using the Taguchi method. The signal-to-noise ratio (S/N) is a measure of robustness, which can be used to identify the control factor settings that minimize the effect of noise on the response. S/N was calculated for each factor level combination. The formula for the larger-is-better S/N is shown in (1) [25]:

$$S/N = -10 \times \log(\sum (1/Y^2)/n) \quad (1)$$

where Y represents the given factor level combination and n is the number of responses in the combination. The significance of the RSW parameters was adjusted by performing an ANOVA of the pull-cut results. ANOVA is a statistical process that can be implemented in the results of RSW samples to show the contribution of each variable in the RSW process according to a certain confidence level. Different orthogonal arrays are available depending on the number and degree of process parameters. The analysis was achieved by choosing the correct orthogonal sequence for the current process.

III. RESULTS AND DISCUSSION

A. Microstructure

Figure 2 shows an example of the RSW nuggets and microstructures formed at minimum weld current and weld pressure of 4 kA and 3.5 bar, respectively. The weld nugget contains Heat Affected Zone (HAZ), melting, and temperature zones exceeding Ac_3. As shown in Figure 2, the weld metal structure is composed of a martensite phase, residual maybe 2-9%, excluding austenite detection as it requires a detailed study. The RSW center can heat up to approximately 1900 °C during the process, but this is local heating. The farther away from the weld center, the lower the temperature. In this way, a temperature gradient is formed from the center of the weld to the base metal. A weld zone is formed as metal melts and solidifies (fusion) in a region defined as nugget, HAZ, and base metal regions. Thus, RSW forms three different zones in the weld areas. The austenite forming in the weld metal and HAZ during rapid cooling by electrode water transforms to martensite, but this depends on the hardenability properties of the materials. Due to the high hardenability of general AHSS, dual-phase steel is like the one in this study, and martensite formation can easily be observed.

HAZ can be divided into martensite and dual-phase zones. In the first region, during RSW, the temperature is between the melting point and the A3 temperatures, thus, austenite was formed. On the other hand, at temperatures between A3 and A1 terminal arrest, austenite transforms into ferrite. In both the austenite and ferrite phases, there is a two-phase change amount according to the top and holding times.

Consequently, two zones of austenites transform to martensite during cooling after the RWS cuts off the electricity. These structures can be seen clearly in Figure 2. According to [26-27], the heterogeneous microstructures formed by the RSW process could be explained this way. In addition, the columnar structures elongate in a direction parallel to the electrode force. It could be estimated that the microstructure was more heterogeneous in HAZ than in the weld nugget. The grains of the superheated central zone mainly contain coarse martensite [27-29]. According to [27, 30], this is due to the high hardenability of DP steels, primarily due to high Mn and other alloying elements, despite the low carbon ratio. Moreover, this hardenability strictly depends on external cooling conditions. In force applications, the damage of RSW welded joints of DP steels mainly occurs in the softening zone under the tempering effect in the HAZ or the base material bordering this zone. This issue is more sensitive, especially in high-carbon and high-strength DP steels.

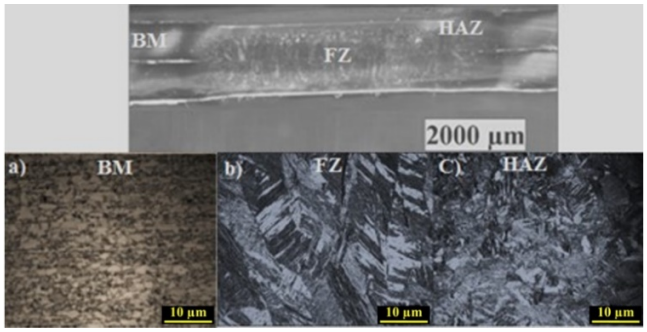

Fig. 2. Macrostructure and microstructure of DP600 RSW sample welded with 4 kA - 3.5 bar: a) Base Metal (BM), b) Fusion Zone (FZ), c) Heat Affected Zone (HAZ).

B. Nugget Formation

Previous studies have experimentally investigated nugget formation throughout the RSW. Weld strength is the most important feature that determines the weld quality of RSW specimens, which largely depends on the geometry and dimensions of the nuggets [31]. Therefore, it is essential to understand the geometry and dimensions of the nuggets [3, 32-34]. Table III shows the results. The most oversized nugget diameter was obtained at 8.25 mm, and this result can be accepted for the base metal in the scope of the $5\sqrt{t}$ rule, where t is the thickness of the material [27]. Different studies have reported different ranges for nugget diameter. Nugget diameter was in the range of 6.35-8.95 mm in [35], approximately in the range of 3-8 mm in [36], approximately 7.0 mm in [37], 2.97-7.14 mm in [16], and 4.8-5.58 mm in [38]. Compatible values could be observed when comparing these results with the ones of this study. On the other hand, differences in the results can be attributed to welding parameters, electrode tip type, electrode tip diameters, and so on. Furthermore, nugget formation depends on welding time, welding current, other periods, welding pressure, and cooling phenomenon [3, 32]. According to [3], RSW nugget formation can be studied in three phases: recovery and progression, growth, and reaching equilibrium. During the rapid, typically shorter than one cycle, development phase, nugget forms due to the metal melting on the metal resistance. The nugget overmagnifies its grade faults during development, occurring over 0.04-0.08 s. Eventually, nugget development completes after about 0.08 s [39].

The weld current and time increase the dimensions of the nugget caused by increasing weld heat input [3, 38, 40]. However, increasing the electrode clamping pressure reduces electrical resistance. Thus, the heat generated at the interface is reduced, resulting in a smaller nugget size [3, 31, 40]. Table III shows that the diameter of the nugget increases with increasing current and decreases with increasing electrode clamping pressure. Table III also shows that an increase in time increases both the penetration rate of the welding and the diameters of the nugget at a constant electrode pressure and increased welding current. Therefore, it could be deduced that the nugget fusion zone size increases with the highest load, indentation ratio, and failure force. In [41], it was reported that there is an essential relationship between weld nugget dimensions, tensile shear load-bearing capacity, and tensile fracture energy.

TABLE III. CHANGE OF NUGGET WITH DIFFERENT WELDING PARAMETERS

Electrode clamping pressure (bar)	Welding current (kA)	Nugget diameter (mm)	
		0.5s	**0.3s**
3.5	4	5.52	4.62
	6	6.15	5.87
	8	8.25	7.67
4.5	4	4.85	4.08
	6	5.73	5.52
	8	7.80	7.55
5.5	4	4.45	3.82
	6	5.64	5.24
	8	7.50	7.31

C. TLBC vs Weld Current via Electrode Clamping Pressure

Figure 3 shows the results of the tensile shear tests. In general, increasing the electrode clamping pressure decreased the TLBC value for both weld time group samples. For example, samples with 4 kA weld current and 0.5 s weld time indicated that TLBC decreases by 0.0178 when the electrode's clamping pressure increases from 3.5 to 4.5 bar. TLBC decreases by 0.052 when electrode clamping pressure increases from 3.5 to 5.5 bar. Furthermore, when the electrode clamping pressure increases from 4.5 to 5.5 bar, the TLBC decreases by 0.0033. A similar trend is also noticed when using 6 kA weld current and 0.5 s weld time. Moreover, the TLBC values of 0.3 s weld time samples have more gaps than the 0.5 s weld time samples. However, increasing the weld current also increased the gap between the highest and lowest TLBC values, according to the weld current and electrode clamping pressures. In addition, 8 kA with a 3.5 bar provided the optimal value for 0.5 s samples. In [1, 11, 42-43], it was noticed that an increase

in welding current increased TLBC for RSW of various metals. The highest TLBC values obtained at 8 kA - 3.5 bar in the literature were 17.76 [16], 16.67 [35], and 13.69 kN [36]. The highest TLBC value was reported in [16] for similar weld current and electrode pressure values for DP600. Therefore, the differences observed in the maximum TLBC values can be attributed to differences in the chemical composition of the steel samples and their sheet thickness. In that respect, this study's TLBC values could be seen as being close to [16].

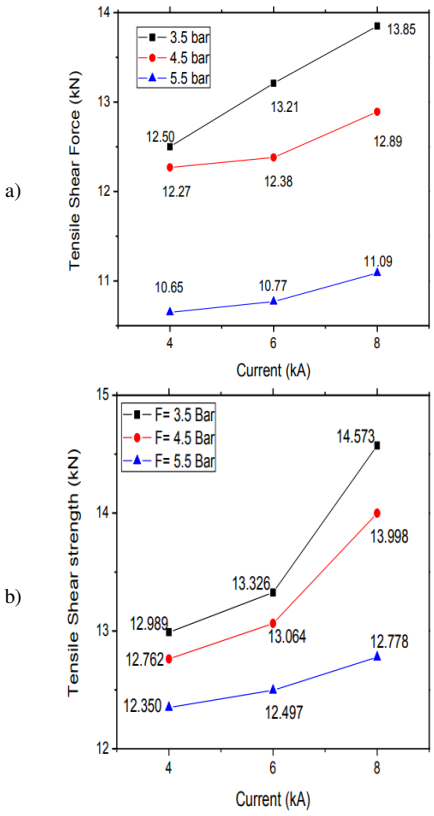

Fig. 3. Current influence on tensile shear load-bearing capacity in different parameters at a) 0.3 s and b) 0.5 s welding time.

D. Taguchi Analysis for TLBC

The optimum joint values were determined for the maximum tensile shear strength. Depending on the experiments, the 8 kA - 0.5 s - 3.5 bar set of values achieved the optimum results. In [38], weld time was found to influence TLBC due to the joule effect. If weld time increases, the TLBC of the specimen increases due to the increased nugget diameter. Table IV and Figure 4 demonstrate the results of the Taguchi analysis. The optimal value of S/N was 22.69 for force level 1. The Taguchi method results from Minitab were compatible with the experimental results. The optimal S/N values obtained from other studies were 16.18 for force level 2 [21], 16.70 for force level 2 [14], and 9.37 and 19.53 for force level 2 and 1 and 2 mm thickness, respectively [15]. This study obtained higher S/N ratios than the others examined. Higher S/N values are known to define control factor settings that minimize the effects of noise factors.

TABLE IV. RESPONSE ANALYSIS FOR S/N RATIOS

Level	F	I
1	22.69	22.08
2	22.46	22.26
3	21.98	22.78

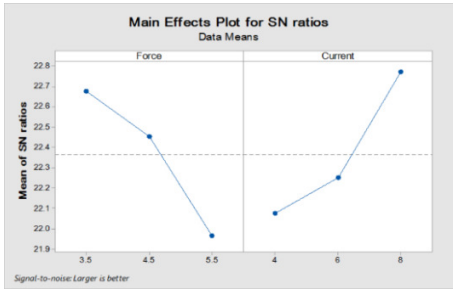

Fig. 4. The main response effects plot of parameters for S/N.

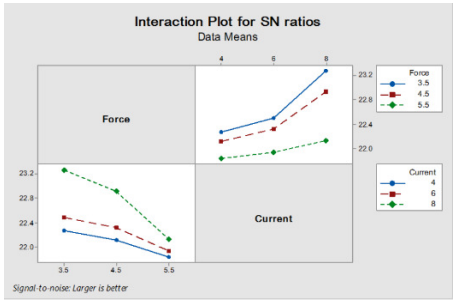

Fig. 5. Interaction of the effect of force and current on S/N.

TABLE V. INFLUENCE OF PARAMETERS ON S/N

Force	Current	TLBC	S/N ratio
3.5	4	12.979	22.271
3.5	6	13.316	22.495
3.5	8	14.583	23.272
4.5	4	12.772	22.119
4.5	6	13.074	22.323
4.5	8	13.999	22.922
5.5	4	12.351	21.834
5.5	6	12.498	21.937
5.5	8	12.779	22.139

The left side of Figure 5 demonstrates the inverse correlation between force and S/N. Table V shows that the highest S/N value was 23.272 at 3.5 bar – 8 kA and decreased with increasing force to more than 3.5 bar at constant current. The right side of Figure 5 shows the effect of welding current on the S/N. When the welding current increases, the S/N ratio increases at a fixed clamping pressure. However, in [14] the highest value was 18.77, in [21] the highest value was 18.46, and in [15] the highest values were 11.43 and 20.56 for 1 and 2 mm thickness, respectively. Therefore, this study achieved higher S/N results than the reviewed studies.

Higher than Best (HB) includes TLBC and nugget diameter with higher values. Lower than Best (LB) concerns HAZ, for which a lower value is preferred [15]. As seen in Table V, S/N was found to be maximum at maximum tensile strength, and the minimum value of S/N was 21.834 at 4 kA welding current and 5.5 bar. While the tensile shear is minimal, the S/N varies according to the parameters, is directly proportional to the

welding current, and reverses with the clamping pressure after 3.5 bar.

E. ANOVA for TLBC

As shown in Table VI, TLBC results for current welding parameters are more effective than clamping pressure. In [44], the Taguchi method indicated that in order of importance, preheat welding current, preheat welding time, hold time, welding current, and welding time were the key parameters that affected the tensile shear strength. According to ANOVA in [21], the effective parameters for tensile shear strength were welding current, welding time, electrode pressure, and electrode tip diameter. The welding current was the most important factor affecting the tensile strength (68.93%), while the welding time was the second (18.66%). In [14], welding current contributed the most (53.57%), while hold time showed less effect on tensile shear strength. In [15], the welding current was also the most important factor affecting the tensile strength (57.80% for 1 mm and 40.56% for 2 mm of sheet thickness), while the electrode force was the second most important factor (29.22% for 1 mm and 35.42% for 2 mm of sheet thickness). Therefore, the most important parameter affecting TLBC is the welding current. Figure 6 shows the ANOVA results of TLBC for welding current and clamping pressure. The maximum values were obtained at 3.5 bar – 8 kA, and the minimum at 5.5 bar – 4 kA.

TABLE VI. ANOVA FOR TENSILE SHEAR

Source	DF	Seq ss	Adj ss
Force	2	1.84620	1.84710
Current	2	1.91440	1.91530
Total	8	4.16374	4.16464

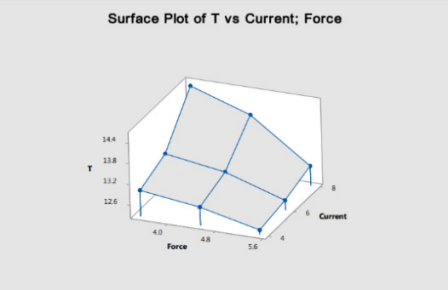

Fig. 6. ANOVA for tensile shear.

IV. CONCLUSION

The following results can be drawn from this study:

- While RSW nugget size and S/N ratio are directly proportional to the welding current and time, they are inversely proportional to the clamping pressure, according to both experimental and statistical analysis.
- TLBC increased in direct proportion to the weld nugget size. The best values of TLBC were estimated for different values of welding parameters and were 8 kA - 3.5 bar.
- The maximum S/N values for TLBC were 22.69 at force level 1 and 22.78 at 8 kA. The maximum and minimum interaction effect values were 23.272 and 21.834 at clamping pressure and welding current of 3.5 and 5.5 bar and 8 and 4 kA, respectively.
- The TLBC results obtained by Taguchi (DOE) and ANOVA showed that the welding current had a stronger effect than the electrode clamping pressure.

ACKNOWLEDGMENT

The authors would like to thank TOFAŞ Inc. in Bursa, Türkiye, for supplying the steel material used in this study. This work was supported by the Scientific Research Projects Coordination Unit of Karabuk University, Türkiye, with project number: KBUBAP-17-KP-463.

REFERENCES

[1] A. Alzahougi, M. Elitas, and B. Demir, "RSW Junctions of Advanced Automotive Sheet Steel by Using Different Electrode Pressures," *Engineering, Technology & Applied Science Research*, vol. 8, no. 5, pp. 3492–3495, Oct. 2018, https://doi.org/10.48084/etasr.2342.

[2] A. R. O. Alzahougi, "Investigation and simulation of resistance spot welding using DP600 steel in automotive industry," Ph.D. dissertation, Karabük University, Karabük, Türkiye, 2020.

[3] M. Pouranvari and S. P. H. Marashi, "Critical review of automotive steels spot welding: process, structure and properties," *Science and Technology of Welding and Joining*, vol. 18, no. 5, pp. 361–403, Jul. 2013, https://doi.org/10.1179/1362171813Y.0000000120.

[4] M. Elitas and B. Demir, "Residual stress evaluation during RSW of DP600 sheet steel," *Materials Testing*, vol. 62, no. 9, pp. 888–890, Sep. 2020, https://doi.org/10.3139/120.111560.

[5] F. Ternane, M. Benachour, F. Sebaa, and N. Benachour, "Regression Modeling and Process Analysis of Resistance Spot Welding on Dissimilar Steel Sheets," *Engineering, Technology & Applied Science Research*, vol. 12, no. 4, pp. 8896–8900, Aug. 2022, https://doi.org/10.48084/etasr.5059.

[6] X. Luo, J. Ren, D. Li, Y. Qin, and P. Xu, "Macro characteristics of dissimilar high strength steel resistance spot welding joint," *The International Journal of Advanced Manufacturing Technology*, vol. 87, no. 1, pp. 1105–1113, Oct. 2016, https://doi.org/10.1007/s00170-016-8581-9.

[7] A. Ramazani, K. Mukherjee, A. Abdurakhmanov, M. Abbasi, and U. Prahl, "Characterization of Microstructure and Mechanical Properties of Resistance Spot Welded DP600 Steel," *Metals*, vol. 5, no. 3, pp. 1704–1716, Sep. 2015, https://doi.org/10.3390/met5031704.

[8] B. Demir, E. Koç, and A. N. Saud, "Effect of Weld Currents on Microstructure, Corrosion Behavior of AZ31 Magnesium Alloy," *Journal of Bio- and Tribo-Corrosion*, vol. 7, no. 2, Feb. 2021, Art. no. 57, https://doi.org/10.1007/s40735-021-00489-5.

[9] M. Elitas and B. Demir, "The Effects of the Welding Parameters on Tensile Properties of RSW Junctions of DP1000 Sheet Steel," *Engineering, Technology & Applied Science Research*, vol. 8, no. 4, pp. 3116–3120, Aug. 2018, https://doi.org/10.48084/etasr.2115.

[10] M. Pouranvari, "Critical assessment 27: dissimilar resistance spot welding of aluminium/steel: challenges and opportunities," *Materials Science and Technology*, vol. 33, no. 15, pp. 1705–1712, Oct. 2017, https://doi.org/10.1080/02670836.2017.1334310.

[11] P. Marashi, M. Pouranvari, S. Amirabdollahian, A. Abedi, and M. Goodarzi, "Microstructure and failure behavior of dissimilar resistance spot welds between low carbon galvanized and austenitic stainless steels," *Materials Science and Engineering: A*, vol. 480, no. 1, pp. 175–180, May 2008, https://doi.org/10.1016/j.msea.2007.07.007.

[12] M. Pouranvari, S. Sobhani, and F. Goodarzi, "Resistance spot welding of MS1200 martensitic advanced high strength steel: Microstructure-properties relationship," *Journal of Manufacturing Processes*, vol. 31, pp. 867–874, Jan. 2018, https://doi.org/10.1016/j.jmapro.2018.01.009.

[13] B. V. H. Hernandez, M. L. Kuntz, M. I. Khan, and Y. Zhou, "Influence of microstructure and weld size on the mechanical behaviour of

dissimilar AHSS resistance spot welds," *Science and Technology of Welding and Joining*, vol. 13, no. 8, pp. 769–776, Nov. 2008, https://doi.org/10.1179/136217108X325470.

[14] A. G. Thakur and V. M. Nandedkar, "Optimization of the Resistance Spot Welding Process of Galvanized Steel Sheet Using the Taguchi Method," *Arabian Journal for Science and Engineering*, vol. 39, no. 2, pp. 1171–1176, Feb. 2014, https://doi.org/10.1007/s13369-013-0634-x.

[15] Uğur Eşme, "Application of Taguchi Method for the Optimization of Resistance Spot Welding Process," *Arabian Journal for Science & Engineering*, vol. 34, no. 2B, pp. 519–528.

[16] D. Zhao, Y. Wang, D. Liang, and P. Zhang, "An investigation into weld defects of spot-welded dual-phase steel," *The International Journal of Advanced Manufacturing Technology*, vol. 92, no. 5, pp. 3043–3050, Sep. 2017, https://doi.org/10.1007/s00170-017-0398-7.

[17] M. Elitas, "Effects of welding parameters on tensile properties and fracture modes of resistance spot welded DP1200 steel," *Materials Testing*, vol. 63, no. 2, pp. 124–130, Feb. 2021, https://doi.org/10.1515/mt-2020-0019.

[18] M. Eshraghi, M. A. Tschopp, M. Asle Zaeem, and S. D. Felicelli, "Effect of resistance spot welding parameters on weld pool properties in a DP600 dual-phase steel: A parametric study using thermomechanically-coupled finite element analysis," *Materials & Design (1980-2015)*, vol. 56, pp. 387–397, Apr. 2014, https://doi.org/10.1016/j.matdes.2013.11.026.

[19] X. Q. Zhang, G. L. Chen, and Y. S. Zhang, "Characteristics of electrode wear in resistance spot welding dual-phase steels," *Materials & Design*, vol. 29, no. 1, pp. 279–283, Jan. 2008, https://doi.org/10.1016/j.matdes.2006.10.025.

[20] H. Aydin, "The mechanical properties of dissimilar resistance spot-welded DP600–DP1000 steel joints for automotive applications," *Proceedings of the Institution of Mechanical Engineers, Part D: Journal of Automobile Engineering*, vol. 229, no. 5, pp. 599–610, Apr. 2015, https://doi.org/10.1177/0954407014547749.

[21] A. G. Thakur, T. E. Rao, M. S. Mukhedkar, and V. M. Nandedkar, "Application of Taguchi Method for Resistance Spot Welding of Galvanized Steel," *ARPN Journal of Engineering and Applied Sciences*, vol. 5, no. 11, pp. 22–26, Nov. 2010.

[22] M. Pouranvari and S. P. H. Marashi, "Key factors influencing mechanical performance of dual phase steel resistance spot welds," *Science and Technology of Welding and Joining*, vol. 15, no. 2, pp. 149–155, Feb. 2010, https://doi.org/10.1179/136217109X12590746472535.

[23] X. Wan, Y. Wang, and P. Zhang, "Modelling the effect of welding current on resistance spot welding of DP600 steel," *Journal of Materials Processing Technology*, vol. 214, no. 11, pp. 2723–2729, Nov. 2014, https://doi.org/10.1016/j.jmatprotec.2014.06.009.

[24] D. Zhao, Y. Wang, D. Liang, and P. Zhang, "Modeling and process analysis of resistance spot welded DP600 joints based on regression analysis," *Materials & Design*, vol. 110, pp. 676–684, Nov. 2016, https://doi.org/10.1016/j.matdes.2016.08.038.

[25] "Minitab 18 Support," Minitab LLC, 2019.

[26] S. T. Wei *et al.*, "Similar and dissimilar resistance spot welding of advanced high strength steels: welding and heat treatment procedures, structure and mechanical properties," *Science and Technology of Welding and Joining*, vol. 19, no. 5, pp. 427–435, Jul. 2014, https://doi.org/10.1179/1362171814Y.0000000211.

[27] B. Demir and M. Erdoğan, "The hardenability of austenite with different alloy content and dispersion in dual-phase steels," *Journal of Materials Processing Technology*, vol. 208, no. 1, pp. 75–84, Nov. 2008, https://doi.org/10.1016/j.jmatprotec.2007.12.094.

[28] B. Demir and M. Erdogan, "Tensile Properties of the Hardenable Dual Phase Steel with Different Martensite Dispersion," *JESTECH*, vol. 15, no. 1, pp. 13–19, 2012.

[29] B. Demir and M. Erdogan, "Fracture Behavior of the Hardenable Dual Phase Steel with Different Martensite Dispersions," *JESTECH*, vol. 15, no. 2, pp. 97–103, 2012.

[30] M. Amirthalingam, E. M. van der Aa, C. Kwakernaak, M. J. M. Hermans, and I. M. Richardson, "Elemental segregation during resistance spot welding of boron containing advanced high strength steels," *Welding in the World*, vol. 59, no. 5, pp. 743–755, Sep. 2015, https://doi.org/10.1007/s40194-015-0250-3.

[31] K. Zhou and L. Cai, "Study on effect of electrode force on resistance spot welding process," *Journal of Applied Physics*, vol. 116, no. 8, Aug. 2014, Art. no. 084902, https://doi.org/10.1063/1.4893968.

[32] F. Hayat, B. Demir, M. Acarer, and S. Aslanlar, "Effect of weld time and weld current on the mechanical properties of resistance spot welded IF (DIN EN 10130–1999) steel," *Kovove Materialy*, vol. 47, no. 1, pp. 11–17, 2009.

[33] X. Sun, E. V. Stephens, and M. A. Khaleel, "Effects of fusion zone size and failure mode on peak load and energy absorption of advanced high strength steel spot welds under lap shear loading conditions," *Engineering Failure Analysis*, vol. 15, no. 4, pp. 356–367, Jun. 2008, https://doi.org/10.1016/j.engfailanal.2007.01.018.

[34] M. Pouranvari, H. R. Asgari, S. M. Mosavizadch, P. H. Marashi, and M. Goodarzi, "Effect of weld nugget size on overload failure mode of resistance spot welds," *Science and Technology of Welding and Joining*, vol. 12, no. 3, pp. 217–225, Apr. 2007, https://doi.org/10.1179/174329307X164409.

[35] C. Ma, D. L. Chen, S. D. Bhole, G. Boudreau, A. Lee, and E. Biro, "Microstructure and fracture characteristics of spot-welded DP600 steel," *Materials Science and Engineering: A*, vol. 485, no. 1, pp. 334–346, Jun. 2008, https://doi.org/10.1016/j.msea.2007.08.010.

[36] M. I. Khan, M. L. Kuntz, E. Biro, and Y. Zhou, "Microstructure and Mechanical Properties of Resistance Spot Welded Advanced High Strength Steels," *Materials Transactions*, vol. 49, no. 7, pp. 1629–1637, 2008, https://doi.org/10.2320/matertrans.MRA2008031.

[37] X. Long and S. K. Khanna, "Fatigue properties and failure characterization of spot welded high strength steel sheet," *International Journal of Fatigue*, vol. 29, no. 5, pp. 879–886, May 2007, https://doi.org/10.1016/j.ijfatigue.2006.08.003.

[38] R. Kumar, J. S. Chohan, R. Goyal, and P. Chauhan, "Impact of process parameters of resistance spot welding on mechanical properties and micro hardness of stainless steel 304 weldments," *International Journal of Structural Integrity*, vol. 12, no. 3, pp. 366–377, Jan. 2020, https://doi.org/10.1108/IJSI-03-2020-0031.

[39] S. Aslanlar, A. Ogur, U. Ozsarac, and E. Ilhan, "Welding time effect on mechanical properties of automotive sheets in electrical resistance spot welding," *Materials & Design*, vol. 29, no. 7, pp. 1427–1431, Jan. 2008, https://doi.org/10.1016/j.matdes.2007.09.004.

[40] A. Alzahougi, M. Elitaş, and B. Demir, "The Relationship of the Force Effect with the Effect of Current on Weld Quality in Resistance Spot Welding," presented at the UDCS'19 Fourth International Iron and Steel Symposium, Karabük, Türkiye, Apr. 2019, pp. 114–117.

[41] H. Zhang, A. Wei, X. Qiu, and J. Chen, "Microstructure and mechanical properties of resistance spot welded dissimilar thickness DP780/DP600 dual-phase steel joints," *Materials & Design (1980-2015)*, vol. 54, pp. 443–449, Feb. 2014, https://doi.org/10.1016/j.matdes.2013.08.027.

[42] D. Q. Sun, B. Lang, D. X. Sun, and J. B. Li, "Microstructures and mechanical properties of resistance spot welded magnesium alloy joints," *Materials Science and Engineering: A*, vol. 460–461, pp. 494–498, Jul. 2007, https://doi.org/10.1016/j.msea.2007.01.073.

[43] S. Fukumoto, K. Fujiwara, S. Toji, and A. Yamamoto, "Small-scale resistance spot welding of austenitic stainless steels," *Materials Science and Engineering: A*, vol. 492, no. 1, pp. 243–249, Sep. 2008, https://doi.org/10.1016/j.msea.2008.05.002.

[44] R. Neystani, B. Beidokhti, and M. Amelzadeh, "Fabrication of dissimilar Fe-Cu-C powder metallurgy compact/steel joint using the optimized resistance spot welding," *Journal of Manufacturing Processes*, vol. 43, pp. 200–206, Jul. 2019, https://doi.org/10.1016/j.jmapro.2019.05.014.